

# Lab on a Chip

Accepted Manuscript



This is an *Accepted Manuscript*, which has been through the Royal Society of Chemistry peer review process and has been accepted for publication.

*Accepted Manuscripts* are published online shortly after acceptance, before technical editing, formatting and proof reading. Using this free service, authors can make their results available to the community, in citable form, before we publish the edited article. We will replace this *Accepted Manuscript* with the edited and formatted *Advance Article* as soon as it is available.

You can find more information about *Accepted Manuscripts* in the [Information for Authors](#).

Please note that technical editing may introduce minor changes to the text and/or graphics, which may alter content. The journal's standard [Terms & Conditions](#) and the [Ethical guidelines](#) still apply. In no event shall the Royal Society of Chemistry be held responsible for any errors or omissions in this *Accepted Manuscript* or any consequences arising from the use of any information it contains.

## ARTICLE

Cite this: DOI: 10.1039/x0xx00000x

Received 00th January 2012,  
Accepted 00th January 2012

DOI: 10.1039/x0xx00000x

[www.rsc.org/](http://www.rsc.org/)

# A Handheld Flow Genetic Analysis System (FGAS): Towards Rapid, Sensitive, Quantitative, Multiplex Molecular Diagnosis at the Point-of-Care Level

Bowen Shu, Chunsun Zhang\* and Da Xing\*

A handheld flow genetic analysis system (FGAS) is proposed for rapid, sensitive, multiplex, real-time quantification of nucleic acids at the point-of-care (POC) level. The FGAS includes a helical thermal-gradient microreactor and a microflow actuator, as well as control circuitry for temperature, fluid, and power management, and smartphone fluorescence imaging. All of these features are integrated into a field-portable and easy-to-use molecular diagnostic platform powered by lithium batteries. Due to the unique design of the microreactor, not only steady temperatures for denaturation, annealing/extension but also a linear thermal gradient for spatial high-resolution melting can be achieved through simply maintaining a single heater at constant temperature. The smartphone fluorescence imaging system has a wide field of view that captures all PCR channels of the microreactor in a single snapshot, without the need for any mechanical scanning. By these designs, the FGAS enables real-time monitoring of the temporal and spatial fluorescence signatures of amplicons during continuous-flow amplification. On the current FGAS, the FGAS detection of as little as 10 copies/ $\mu\text{L}$  genomic DNA of *Salmonella enteric* was achieved in 15 min, with real-time quantitative detection of the DNA over 6 orders of magnitude concentration from  $10^6$  to  $10^1$  copies/ $\mu\text{L}$  could also be completed in 7.5-15 min. In addition, multiple pathogenic DNA targets could be simultaneously discriminated with direct bar-chart readout or multiplex spatial melting in a serial flow. We anticipate that the FGAS has the great potential to become a next-generation gene analyzer for POC molecular diagnostics.

## 1. Introduction

Point-of-care (POC) genetic analysis is already of great importance in applications in disease diagnosis, pathogen detection, and forensic identification<sup>1-3</sup>. In these applications, the ideal tool for genetic analysis must be portable, rapid and sensitive. Moreover, it is critical to enable real-time, quantitative and multiplex identification across a wide dynamic range, in order to provide the target information that traditional end-point methods of detection fail to provide. For example, in many cases the presence of a biomarker does not suggest the occurrence of disease unless its concentration is above a diagnostic threshold or several related biomarkers are confirmed<sup>4, 5</sup>. To this end, a microfluidic system combined with real-time nucleic acid amplification has potential to offer desirable features for POC genetic analysis.

Improvements over the past two decades have brought forth several molecular technology platforms for microfluidic real-time nucleic acid analysis, including isothermal amplification systems, temporal polymerase chain reaction (PCR) systems and spatial (or continuous-flow) PCR systems. For isothermal

amplification systems, quantitative ability, accuracy and sensitivity critically rely on the duration of the time-based assays<sup>6</sup>, which largely limits the speed of analysis, especially in the case of low-abundance analytes. In addition, the robust detection of products remains analytically difficult. The most used detection methods (e.g. dye staining or solution turbidity) allow for real-time monitoring of signals but sacrifice specificity, because any accumulation of nonspecific or parasitic amplicons yields a false-positive signal<sup>7</sup>. For temporal PCR systems, precise and repeated thermal cycling often leads to excessive time and power consumption, complex temperature control, as well as complicated and bulky structure design. Spatial PCR systems circumvent the need for repeated heating and cooling of the reaction chamber of the temporal ones by moving the sample through alternating temperature zones, thus alleviating such shortcomings of temporal PCR systems.

The spatial PCR concept of using a capillary passing through various temperature baths was demonstrated by Nakano et al. in 1994<sup>8</sup>. In 1998, Manz and co-workers

developed a spatial PCR chip using a serpentine channel passing through three temperature zones<sup>9</sup>. Since then, especially during the last decade, such PCR microfluidic technologies have made great advances, such as using a capillary and a cylindrical heating-block assembly to construct a compact spatial PCR device<sup>10</sup>, using continuous segmented-flow PCR for high-throughput DNA amplification<sup>11</sup>, performing contamination-free spatial PCR using isolated droplets flowing in an immiscible fluorinated solvent system<sup>12</sup>, integrating end-point<sup>11, 13</sup> or real-time<sup>14-16</sup> fluorescence detection onto spatial PCR, injecting oil in spatial PCR to circumvent air bubbles<sup>17</sup>, doing spatial PCR with just one heater<sup>18-20</sup>, simultaneously performing spatial PCR and melting analysis with linear temperature gradients<sup>21</sup>, and determining real-time spatial PCR curves by analyzing a single fluorescent image<sup>22</sup>. So far, however, almost all spatial PCR systems are far from POC use, because they still rely on bulky off-chip infrastructures (e.g., pumping sources, computers, detection instruments and power supply). These limitations ultimately prevent their wide-spread adoption.

In this study, we have developed the handheld flow genetic analysis system (FGAS)—an integrated microfluidic platform for rapid, sensitive, quantitative, multiplex analysis of specific DNA targets. To achieve this, the presented system has some distinct features: (1) a helical thermal-gradient single heater microreactor is designed to provide steady temperatures for spatial PCR amplification as well as a linear thermal gradient for spatial high resolution melt (SHRM) analysis; (2) a smartphone fluorescence imaging system with a large field of view, which enables all channels of the microreactor to be imaged in a single image without mechanical scanning. This feature is used to monitor the temporal and spatial fluorescence signatures throughout the PCR process in real time; and (3) it has other infrastructures (including microflow actuator, electronics for control of temperature, fluid and power, as well lithium battery) self-contained to create an ultra-compact, battery-powered and easy-to-operate molecular diagnosis platform. To evaluate the effectiveness of the FGAS, three representative pathogens—*Salmonella enterica*, *Listeria monocytogenes* and *Staphylococcus aureus* that often cause food poisoning, were tested. This handheld platform, along with a novel fluid operation protocol, exhibits the ability of high-speed quantification, the versatility of specific and sensitive assay, and the potential for multiplex, high-throughput application.

## 2. Experimental

### 2.1. Design of the FGAS

The assembled hand-held FGAS, as shown in **Figure 1a**, measures 15 cm × 10 cm × 12 cm. It consists of five subsystems (**Figure 1b and c**) for: thermal-gradient microreactor, smartphone fluorescence imaging, self-containing microflow actuator, electronics for temperature, fluid and power management, and lithium battery. Two key subsystems

are described in detail as follow, and the descriptions of other subsystems can be found in the Electronic Supplementary Information (ESI).

The thermal-gradient element of the microreactor (35 mm × 45 mm × 10 mm) was formed by an applanate “C”-shaped brass block on whose surface the helical U-shaped grooves (0.6 mm × 0.6 mm) were machined. As depicted in **Figure 1c**, the hot side houses a cartridge heater (6.8 Ω, 4 mm × 50 mm [o.d. × length]) to maintain a denaturation temperature. And, this heater is regulated by a fuzzy PID temperature controller with an accuracy of ± 0.1 °C, which is included in the electronic subsystem. The cooling side of the brass block is connected to a copper heat sink, and this heat sink can be cooled by simply regulating the applied voltage of the micro-fan. These two elements work together to obtain variable annealing conditions. A transparent thin-wall polytetrafluoroethylene (PTFE) capillary tube (0.3 mm × 0.6 mm × 3500 mm, i.d. × o.d. × length) was wrapped forty-two turns around the grooves, with 78.4 mm length tube per cycle. During the development of the microreactor, a high-precision PCI-4351 data acquisition card (National Instruments, Austin, TX, USA) connected to K-type thermocouples was used to characterize its thermal response and spatial temperature distribution.

As illustrated in **Figure 1c**, the Smartphone fluorescence imaging system consists of a high-intensity light emitting diode (LED) with a dominant wavelength at 475 nm (XRE-B4, Cree, Inc., USA), a commercial fluorescence filter set (AF002, HB Optical Technology Co., Ltd., China), and a smartphone (Mi One, Xiaomi Inc., China). The excitation light from the LED, which is filtered by a 455-495 nm band-pass excitation filter and laterally reflected at 90° by a long-pass dichroic mirror with a cut-off wavelength of 501 nm, was used to excite the EvaGreen® Dye (Biotium, Inc., USA) in the PCR mixture. The fluorescence during spatial PCR reaction was collected through the same dichroic mirror, passed through a band-pass emission filter with a center wavelength of 535 nm and bandwidth of 45 nm, and detected by a complementary metal-oxide semiconductor (CMOS) camera (f/2.4, 8 megapixel) on the smartphone. The imaging module was placed 5 cm above the thermal-gradient microreactor, with an effective imaging area of ~ 4.5 cm<sup>2</sup>. To obtain a fixed imaging boundary, an aluminium sheet with a rectangular opening (45 mm × 25 mm) was used as the detection window. Benefiting from the large field-of-view imaging and the unique design of microreactor, the image covering 42 PCR channels could be captured in a single snapshot, without any mechanical movement of the microreactor or the imaging system. As an alternative to visual analysis, the captured fluorescence images can be transmitted wirelessly (or by USB cable) to our servers that can rapidly process these images to produce amplification curves and melting curves.

### 2.2. Fluid operation protocol

Prior to sample loading, the samples were prepared in separated PCR tubes, and each was covered with 10 μL light mineral oil.

To reduce bubble formation in the sample solution, a small plug of mineral oil (~10  $\mu\text{L}$ ) was first introduced into the reaction channel. Then, the sample plug was pumped through the reaction tube at a linear flow rate of 4 mm/s. Here, the sample plug was generated by simply aspirating defined volumes of aqueous solution and mineral oil into the reaction channel, similar to the procedure reported in our recent work<sup>23, 24</sup>. Initially, the aspirating tip was moved into the oil layer, and about 5  $\mu\text{L}$  of mineral oil was taken. Subsequently, the tip was continuously moved to the bottom of sample solution, and 10- $\mu\text{L}$  sample solution was taken followed by the 5- $\mu\text{L}$  oil. In the case of serial analysis, the tip was moved into the oil layer of the next sample tube, and the above operations were repeated to produce another sample plug. As a result, multiple sample plugs could be formed in the same way.

### 2.3. PCR and spatial melting

Unless otherwise indicated, PCR was performed in 10  $\mu\text{L}$  reaction volumes containing 1  $\times$  PCR buffer, 200  $\mu\text{M}$  of each dNTP, 0.04 ng/ $\mu\text{L}$  BSA, 400 nM each of the primers, 1  $\times$  EvaGreen® dye, 0.2 unit/ $\mu\text{L}$  of Taq polymerase, and 10<sup>5</sup> copies/ $\mu\text{L}$  of template DNA. More details about the materials and reagents can be seen in the ESI. Unless otherwise stated, continuous-flow PCR was carried out for 42 cycles at 4 mm/s, where a thermal gradient was established by maintaining the heater at 94.0  $^{\circ}\text{C}$  and the applied voltage of the microfan at 3.5 V. Thus, the corresponding residence time in the temperature zone of 90.0-94.0  $^{\circ}\text{C}$  (for denaturation) was 5 s, and that in the temperature zone of 50.3-75.0  $^{\circ}\text{C}$  (for annealing/extension) was about 11 s. For performing spatial real-time PCR and spatial melting, the linear thermal-gradient region (~0.9  $^{\circ}\text{C}/\text{mm}$ ) from 71.8 to 92.7  $^{\circ}\text{C}$  was detected by the smartphone fluorescence imaging.

For comparison, the conventional real-time PCR and high-resolution melting (HRM) on the LightCycler (Roche Applied Science) were also performed. Its amplification protocol included an initial denaturation step of 94.0  $^{\circ}\text{C}$  for 60 s followed by 42 cycles of 94.0  $^{\circ}\text{C}$  for 5 s, 50.3  $^{\circ}\text{C}$  for 5 s, and 75.0  $^{\circ}\text{C}$  for 15 s. After PCR, a denaturation/renaturation step was implemented at 94.0  $^{\circ}\text{C}$  for 3 s and 50.0  $^{\circ}\text{C}$  for 3 s before melting the product. The product was then melted from 72.0  $^{\circ}\text{C}$  to 93.0  $^{\circ}\text{C}$  with a 0.1  $^{\circ}\text{C}/\text{s}$  ramping rate to produce HRM curves.

### 2.4. Fluorescence image acquisition and analysis

In spatial real-time quantitative PCR and HRM, image capture settings were taken at f/2.4 aperture, ISO ~1600, 4 mm focal length, and acquisition rate of 0.1 Hz. The open source ImageJ software (<http://rsb.info.nih.gov/ij/download.html>) was used for image processing and intensity analysis.

A typical amplification curve and its threshold cycle (Ct) value were determined by the following procedure: (1) The acquired images of whole amplification process were aligned in a temporal sequence, and the fluorescent channels were exposed from each other to form a combined fluorescence image. (2) The RGB channels of the combined fluorescence

image were split, with green channel information remained. (3) The intensity of a 100-pixel line width at a vertical position (from the top to the bottom of the image) was plotted. (4) The highest intensity of each channel and the lowest intensity of the region between two neighbouring channels could be dynamically selected by using float cursors. As a result, the fluorescence intensity of the channel could be calculated as the highest intensity of the channel minus the mean of the lowest intensities in these two regions. (5) A plot of fluorescence versus channel (or cycle) number was displayed, with the data points smoothed by a first order Savitzky-Golay filter. (6) The Ct value of the amplification curve was calculated using the second derivative method<sup>25</sup>.

Melting curves were generated using the following steps: Initially, the RGB channels of the interest image were split, with green channel information retained. Subsequently, the background of the image was subtracted, and a 10-pixel-wide horizontal line that almost covered the corresponding fluorescent channel was used to extract the fluorescence intensity. Then, the data points were smoothed with 1-order Savitzky-Golay filter to plot the profile of melting, in which the intensity of fluorescence was measured as a function of pixel. Finally, the pixels were converted to the temperature data ( $T'$ ) according to the spatial temperature resolution ( $^{\circ}\text{C}/\text{pixel}$ ), and the final temperature data were calculated as  $T = T' + T_0$ , where  $T_0$  were the temperatures of the first melting point that were determined by the applied voltage of the microfan (for example,  $T_0$  was 71.8  $^{\circ}\text{C}$  in the case of 3.5 V). Thus, a melting curve was produced, in which fluorescence was measured as a function of temperature.

## 3. Results and discussion

### 3.1. Operation principle of the FGAS

As displayed in **Figure 2**, the FGAS has an architecture with a thermal-gradient microreactor (**a**) coupled with smartphone fluorescence imaging (**b**). Thus, it allows the continuous-flow (spatial) PCR process to be monitored in real time. By simply maintaining a single heater at constant temperature, the microreactor achieves not only desirable temperatures for DNA denaturation and primer annealing/extension, but also a linear thermal gradient for SHRM analysis. When the fluorescence dye-containing mixture flows continuously through the thermal gradient, the fluorescence images are taken sequentially (**c**). The temporal fluorescence information measured along  $x$ -axis, which is comprised of sequential frames, can be used to generate amplification curves (**d**). Meanwhile, the spatial fluorescence information (single frame) (**e**) whose intensity is measured along  $y$ -axis, can be generated to melting curves (**f**).

### 3.2. Evaluation of temperature control and thermal gradient for the microreactor of the FGAS

The design of microreactor was verified by evaluating its temperature control and thermal gradient. In our design, the thermal gradient element was made of the brass substrate,

where the hot side was maintained at 94.0 °C and the cooling side was passively heated by the thermal conduction of the substrate. For compact thermal structure and flexible annealing condition, the temperature of the cooling side should be adjustable. To this end, two kinds of heat-flow regulating methods have been utilized, including passive cooling (e.g. thermal interconnections<sup>26,27</sup>, configuration of heaters<sup>28,29</sup> or reactors<sup>19,20,30</sup>) and active cooling<sup>31-33</sup>. In our case, the voltage-regulated fan and heat sink were incorporated with the single heater microreactor to achieve this. As shown in **Figure 3a**, stable temperatures for PCR were obtained by using a single heater, and varied annealing temperatures from 47.6 to 57.2 °C could be achieved by adjusting the applied voltages from 5.0 V to 2.0 V. Importantly, a good linear thermal gradient was formed for SHRM in the fluorescence detection zone (**Figure 3b and c**). Here, thermal gradients of 0.3-0.9 °C/mm could be well formed along the 25-mm (~1000 pixel) thermal-gradient zone, resulting in a temperature resolution of 0.008-0.023 °C/pixel. This temperature resolution is comparable to those obtained on conventional instruments that typically performed high-resolution melting at 0.01-0.04 °C/s<sup>34</sup>. Furthermore, our SHRM could be performed at 1.2-3.6 °C/s in the presence of 4 mm/s. Such scanning rate is faster than that of a recently reported temporal PCR system with a 0.5 °C/s ramping rate to produce HRM curves<sup>35</sup>.

### 3.3. High-speed, real-time quantitative detection on the FGAS

The capacity of the FGAS for high-speed quantification was demonstrated by performing continuous-flow real-time PCR assays for DNA detection of *Salmonella enteric*. **Figure 4a** shows the combined fluorescence images of amplicons with initial concentrations ranging from 10<sup>6</sup> to 0 copies/μL. Intuitively, higher concentrations of initial DNA template yield the first distinguishable fluorescence at lower cycle channels. For example, the first observable fluorescent channel was around 21<sup>st</sup> cycle for 10<sup>6</sup>-copies/μL DNA. And, 10<sup>1</sup>-copies/μL of DNA gave the first distinguishable fluorescent channel to be around 38<sup>th</sup> cycle. These results imply that direct visual detection of genomic DNA low to 10<sup>1</sup> copies/μL could be completed within 15 min. In addition, only 7.5 min was required for visual detection of 10<sup>6</sup>-copies/μL DNA. To evaluate the accurate quantification ability of the FGAS, the fluorescence intensity peak of each cycling channel in each case of **Figure 4a** was further extracted to produce the amplification curves (**Figure 4b**), and furthermore the performance of the FGAS was compared with that of the LightCycler (**Figure 4c**). As seen from **Figure 4c**, the FGAS and the conventional instrument resulted in a reaction efficiency of 81.0% and 97.6%, respectively. In term of efficiency, the FGAS was 83% as efficient compared to the conventional instrument. This reduced efficiency can be attributed to the reduction of the annealing/extension time by about 50%. In addition, amplification over a range of serially diluted template exhibited good linearity. These results suggest that the FGAS is suitable for quantitative, real-time DNA analysis. Notably, this level of

quantification and speed is superior to or at least comparable to that achievable in many other microfluidic platforms<sup>36</sup>, such as temporal PCR platforms<sup>37-39</sup> and spatial PCR platforms (e.g., spiral-channel spatial PCR<sup>14</sup>, serpentine-channel spatial PCR<sup>17,22,40</sup>, straight-channel oscillatory-flow PCR<sup>15,16,41</sup>, and laminar convection PCR<sup>42</sup>), but in a form that offers an exceptional degree of simplicity, integration, portability, and low-cost.

### 3.4. Spatial melting analysis with direct bar-chart readout for simultaneous identification of multiple pathogenic DNAs

To demonstrate the serial analysis ability of FGAS, the spatial melting analysis with direct bar-chart readout<sup>4,43</sup> was used for simultaneous identification of multiple pathogenic DNAs. Here, three DNAs from *Salmonella enterica* (*Sal*), *Listeria monocytogenes* (*Lis*) and *Staphylococcus aureus* (*Sta*) were used as the model targets, and three pairs of primers (see the ESI) target the *invA*, *hlyA*, and *nuc* gene, respectively. As described in **Figure 5a**, three PCR mixture plugs, with a set of primers and its target genomic DNAs included in each one, are simply generated by sequentially aspirating defined volumes of aqueous solution and mineral oil into the reaction channel. The serial products were melted when they passed the detection zone, thus displaying distinct fluorescent bar-chart (**Figure 5b-“Serial”**) which is similar to that performed individually (**Figure 5b-“Individual”**). By comparing with the virtual temperature ruler, the corresponding melting temperatures of the amplified products were observed at about 83.5, 79.8, and 81.7 °C, respectively. The variation in melting temperature of the serial products ( $\Delta T_m$ ) can be proportional to the height of the bar-chart, due to the good linearity of the thermal gradient cross the fluorescence detection zone. To examine the accuracy of such analysis, the intensity of fluorescent channels was extracted to yield the melting curves (**Figure 5c**) as well as negative derivative plots (**Figure 5d**). And, the corresponding control experiments were also performed on the LightCycler (**Figure 5e and f**). The  $T_m$  values of *Sta*, *Lis* and *Sal* obtained on the FGAS were 79.8±0.1 °C, 81.5±0.3 °C, and 83.4±0.1°C, respectively. And, those analysed on the LightCycler were 80.1 °C, 81.4 °C, and 83.7 °C, respectively. As seen from **Figure 5d and f**, the variations among the melting temperatures or profiles of three products from the FGAS almost agree with those from the control. Thus, the serial spatial melting analysis is capable of accurately identifying the PCR products with bar-chart readout, which enables the FGAS to be more easy to use. Furthermore, due to the convenient continuous flow operation and the universal monochrome fluorescent dye labelling, such serial spatial melting analysis is preferable for high-throughput applications.

### 3.5. Serial, multiplex spatial PCR/melting analysis for high-throughput identification of multiple pathogenic DNAs

To exhibit the potential of high-throughput multiplex assay, the serial continuous-flow multiplex PCR (SCF-MPCR) combined with multiplex spatial melting was carried out. SCF-MPCR has been proposed in our recent work for high-throughput and fast

multiplex DNA amplification<sup>27</sup>. However, time-consuming off-line gel electrophoresis or additional fluorogenic probes together with complicated multi-channel fluorescence detection were still required for detection of the multiplex products. In this work, benefiting from the integrated continuous-flow PCR and spatial melting analysis, the FGAS will enable serial and simultaneous multiplex amplification/detection. As a proof of concept, two PCR mixture plugs were produced serially to detect the targets of “*Lis + Sal*” and “*Sta + Sal*”, and typical image was taken when they experienced around 30 cycles, as shown in **Figure 6a**. An obvious stepwise decrease in fluorescence intensity was observed in amplicons of “*Sta + Sal*”, because of the greater variation in their products’ melting temperatures. The corresponding melting curves (**Figure 6b**) and negative derivative plots (**Figure 6c**) illustrate that duplex amplification and identification were well achieved, and that the specificity of detection was confirmed. **Figure 6c** also shows that there are several tiny peaks around two dominant melting peaks. This is probably because of the relatively high random noise levels resulting from the limited exposure time and the high photo-sensitivity (ISO ~1600) of the smartphone’s camera. Note that we first proposed a multiplex spatial melting analysis for simultaneous detection of multiple targets in a single reaction, further enhancing the detection capability of spatial melting analysis<sup>21, 44, 45</sup> and thus expanding the potential application of the FGAS.

#### 4. Conclusions

In summary, we have described a novel handheld FGAS for rapid, sensitive, quantitative, multiplex, POC molecular diagnosis. By integrating a temperature-gradient microreactor with smartphone fluorescence imaging, the FGAS allows simultaneous spatial amplification and melting analysis. Overall, the FGAS allows visual detection of 10 or more copies/ $\mu\text{L}$  DNA in 15 min, and enables accurate DNA quantification with a dynamic range of six orders of magnitude. Moreover, the spatial melting analysis combined with bar-chart readout or SCF-MPCR can be well used for serial identification of multiple DNAs or for high-throughput multiplex analysis. The current performance and potential for expanded capability lead us to envision the FGAS as a powerful tool for molecular diagnostics at the POC level.

#### Acknowledgements

This work was supported by the National Natural Science Foundation of China (61072030), the National Basic Research Program of China (2010CB732602), the Key Program of NSFC-Guangdong Joint Funds of China (U0931005), the project of Guangzhou science and technology plan 2014 (2014J4100030), and the Scientific Research Foundation of Graduate School of South China Normal University (2013kyjj005).

#### Notes and references

MOE Key Laboratory of Laser Life Science & Institute of Laser Life Science, College of Biophotonics, South China Normal University, Guangzhou 510631 (China)

\*E-mail: zhangcs@sclu.edu.cn, zhangcs\_sclu@126.com (C. S. Zhang);

xingda@sclu.edu.cn (D. Xing)

Electronic Supplementary Information (ESI) available: Materials and reagents; Self-containing microflow actuator; Electronic system. See DOI: 10.1039/b000000x/

- 1 K. Hsieh, A. S. Patterson, B. S. Ferguson, K. W. Plaxco and H. T. Soh, *Angew. Chem. Int. Ed.*, 2012, **51**, 4896-4900.
- 2 N. P. Pai, C. Vadrnais, C. Denking, N. Engel and M. Pai, *PLoS Med.*, 2012, **9**, e1001306.
- 3 A. Niemz, T. M. Ferguson and D. S. Boyle, *Trends biotechnol.*, 2011, **29**, 240-250.
- 4 Z. Zhu, Z. Guan, S. Jia, Z. Lei, S. Lin, H. Zhang, Y. Ma, Z. Q. Tian and C. J. Yang, *Angew. Chem. Int. Ed.*, 2014, **53**, 12503-12507.
- 5 A. M. Foudeh, T. F. Didar, T. Veres and M. Tabrizian, *Lab Chip*, 2012, **12**, 3249-3266.
- 6 H. Noh and S. T. Phillips, *Anal. Chem.*, 2010, **82**, 8071-8078.
- 7 Y. Jiang, B. Li, J. N. Milligan, S. Bhadra and A. D. Ellington, *J. Am. Chem. Soc.*, 2013, **135**, 7430-7433.
- 8 H. Nakano, K. Matsuda, M. Yohda, T. Nagamune, I. Endo and T. Yamane, *BioSci. Biotechnol. Biochem.*, 1994, **58**, 349-352.
- 9 M. U. Kopp, A. J. De Mello and A. Manz, *Science*, 1998, **280**, 1046-1048.
- 10 N. Park, S. Kim and J. H. Hahn, *Anal. Chem.*, 2003, **75**, 6029-6033.
- 11 M. Curcio and J. Roeraade, *Anal. Chem.*, 2003, **75**, 1-7.
- 12 K. D. Dorfman, M. Chabert, J. H. Codarbox, G. Rousseau, P. de Cremoux and J. L. Viovy, *Anal. Chem.*, 2005, **77**, 3700-3704.
- 13 M. Chabert, K. D. Dorfman, P. de Cremoux, J. Roeraade and J.L. Viovy, *Anal. Chem.*, 2006, **78**, 7722-7728.
- 14 A. C. Hatch, T. Ray, K. Lintecum and C. Youngbull, *Lab Chip*, 2014, **14**, 562-568.
- 15 L. Chen, J. West, P.-A. Aurox, A. Manz and P. J. Day, *Anal. Chem.*, 2007, **79**, 9185-9190.
- 16 O. Frey, S. Bonneick, A. Hierlemann and J. Lichtenberg, *Biomed. Microdevices*, 2007, **9**, 711-718.
- 17 T. Nakayama, Y. Kurosawa, S. Furui, K. Kerman, M. Kobayashi, S. R. Rao, Y. Yonezawa, K. Nakano, A. Hino and S. Yamamura, *Anal. Bioanal. Chem.*, 2006, **386**, 1327-1333.
- 18 N. Crews, C. Wittwer and B. Gale, *Proc. SPIE-Int. Soc. Opt. Eng.*, 2007, **6465**, 646504.
- 19 W. Wu, K. T. L. Trinh and N. Y. Lee, *Analyst*, 2012, **137**, 2069-2076.
- 20 W. Wu and N. Y. Lee, *Anal. Bioanal. Chem.*, 2011, **400**, 2053-2060.
- 21 N. Crews, C. Wittwer, R. Palais and B. Gale, *Lab chip*, 2008, **8**, 919-924.
- 22 I. Pjescic, C. Tranter, P. L. Hindmarsh and N. D. Crews, *Biomed. Microdevices*, 2010, **12**, 333-343.
- 23 B. W. Shu, C. S. Zhang and D. Xing, *Anal. Chim. Acta*, 2014, **826**, 51-60.
- 24 C. S. Zhang, H. Y. Wang and D. Xing, *Biomed. Microdevices*, 2011, **13**, 885-897.

- 25 V. Luu-The, N. Paquet, E. Calvo and J. Cumps, *Biotechniques*, 2005, **38**, 287-293.
- 26 N. Agrawal, Y. A. Hassan and V. M. Ugaz, *Angew. Chem. Int. Ed.*, 2007, **46**, 4316-4319.
- 27 K. T. L. Trinh, W. Wu and N. Y. Lee, *Sens. Actuators B-Chem.*, 2014, **190**, 177-184.
- 28 J. Y. Cheng, C. J. Hsieh, Y. C. Chuang and J. R. Hsieh, *Analyst*, 2005, **6**, 931-940.
- 29 N. Crews, C. Wittwer and B. Gale, *Biomed. Microdevices*, 2008, **10**, 187-195.
- 30 W. Wu, K. T. L. Trinha and N. Y. Lee, *Analyst*, 2015, **140**, 1416-1420.
- 31 Y. Schaerli, R. C. Wootton, T. Robinson, V. Stein, C. Dunsby, M. A. Neil, P. M. French, A. J. demello, C. Abell and F. Hollfelder, *Anal. Chem.* 2009, **81**, 302-306.
- 32 C. S. Zhang and D. Xing, *Anal. Biochem.*, 2009, **387**, 102-112.
- 33 T. Ohashi, H. Kuyama, N. Hanafusa and Y. Togawa, *Biomed. Microdevices*, 2007, **9**, 695-702.
- 34 M. G. Herrmann, J. D. Durtschi, C. T. Wittwer and K. V. Voelkerding, *Clin. Chem.*, 2007, **53**, 1544-1548.
- 35 S. O. Sundberg, C. T. Wittwer, R. M. Howell, J. Huuskonen, R. J. Pryor, J. S. Farrar, H. M. Stiles, R. A. Palais and I. T. Knight, *Clin. Chem.*, 2014, **60**, 1306-1313.
- 36 F. Ahmad, S. A. Hashsham, *Anal. Chim. Acta*, 2012, **733**, 1-15.
- 37 N. Ramalingam, H. B. Liu, C. C. Dai, Y. Jiang, H. Wang, Q. H. Wang, K. M. Hui and H. Q. Gong, *Biomed. Microdevices*, 2009, **11**, 1007-1020.
- 38 N. Ramalingam, Z. Rui, H. B. Liu, C. C. Dai, R. Kaushik, B. Ratnaharika and H. Q. Gong, *Sens. Actuator B-Chem.*, 2010, **145**, 543-552.
- 39 R. Zhang, H. Q. Gong, X. D. Zeng and C. C. Sze, *Anal. Bioanal. Chem.*, 2013, **405**, 4277-4282.
- 40 T. H. Fang, N. Ramalingam, X. D. Dong, T. S. Ng, X. T. Zeng, A. T. L. Kuan, E. Y. P. Huat and H. Q. Gong, *Biosens. Bioelectron.*, 2009, **24**, 2131-2136.
- 41 R. Sista, Z. Hua, P. Thwar, A. Sudarsan, V. Srinivasan, A. Eckhardt, M. Pollack and V. Pamula, *Lab Chip*, 2008, **8**, 2091-2104.
- 42 D. Braun, N.L. Goddard and A. Libchaber, *Phys. Rev. Lett.*, 2003, **91**, 158103.
- 43 Y.J. Song, Y.Q. Zhang, P.E. Bernard, J.M. Reuben, N. T. Ueno, R. B. Arlinghaus, Y.L. Zu and L.D. Qin, *Nat. Commun.*, 2012, **3**, 1283.
- 44 N. Crews, C. T. Wittwer, J. Montgomery, R. Pryor and B. Gale, *Anal. Chem.*, 2009, **81**, 2053-2058.
- 45 I. Pjescic and N. Crews, *Lab Chip*, 2012, **12**, 2514-2519.

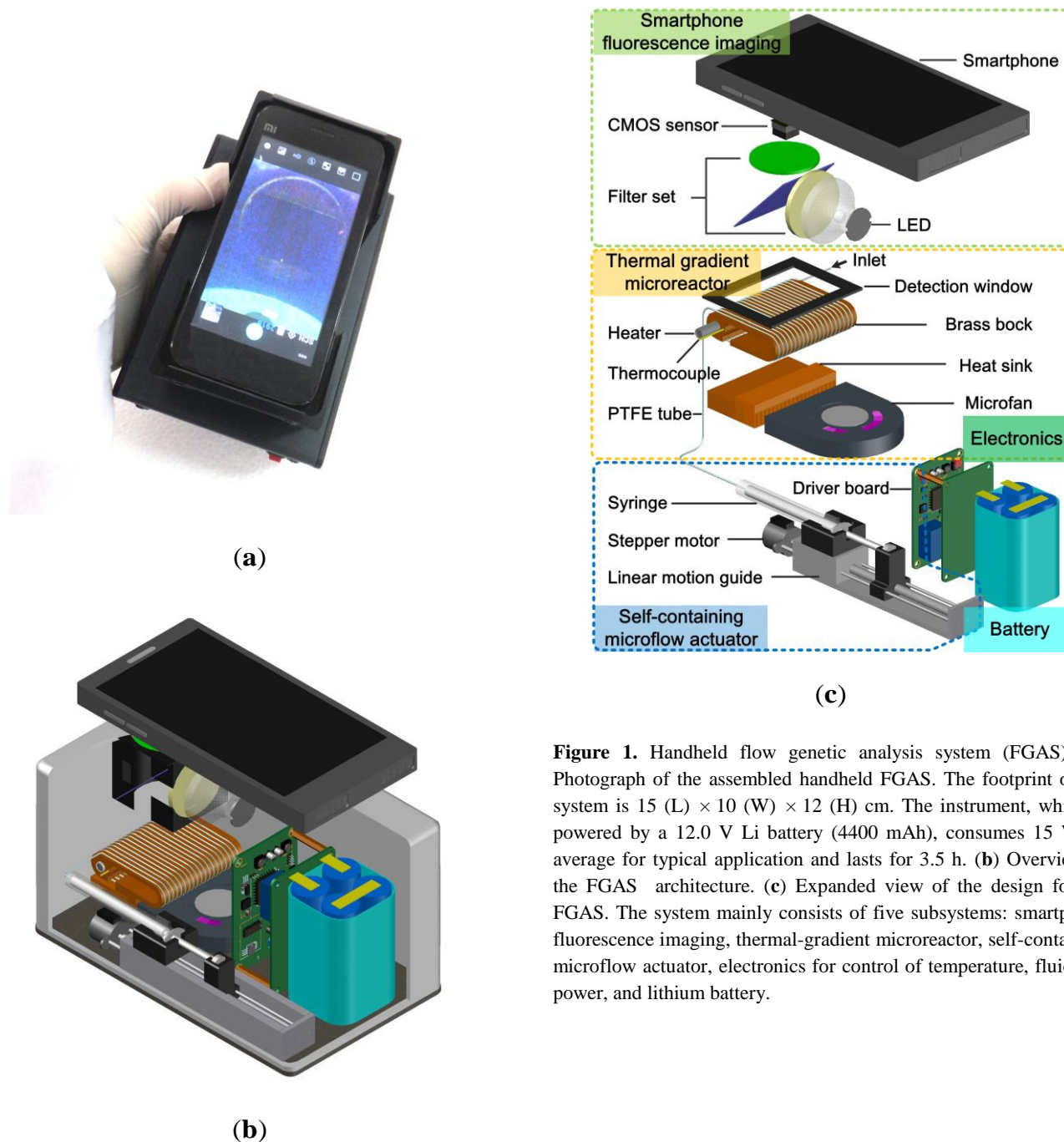


**Figure 1.** Handheld flow genetic analysis system (FGAS). (a) Photograph of the assembled handheld FGAS. The footprint of the system is 15 (L) × 10 (W) × 12 (H) cm. The instrument, which is powered by a 12.0 V Li battery (4400 mAh), consumes 15 W on average for typical application and lasts for 3.5 h. (b) Overview of the FGAS architecture. (c) Expanded view of the design for the FGAS. The system mainly consists of five subsystems: smartphone fluorescence imaging, thermal-gradient microreactor, self-containing microflow actuator, electronics for control of temperature, fluid and power, and lithium battery.

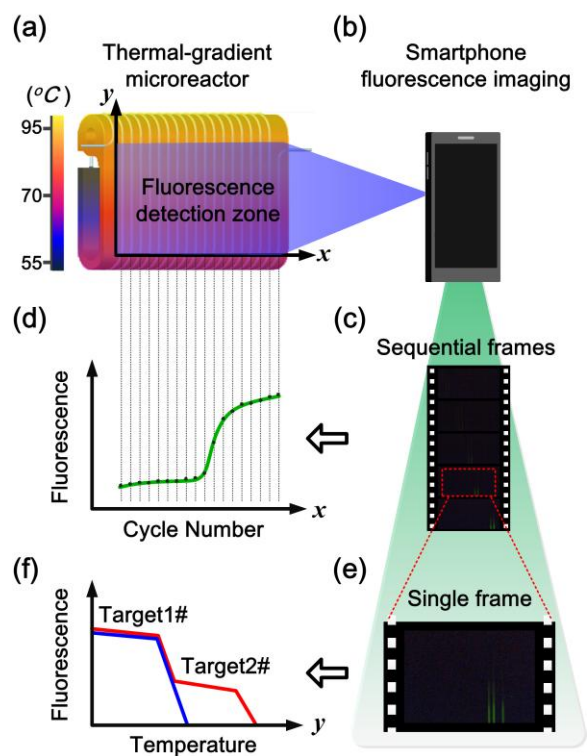
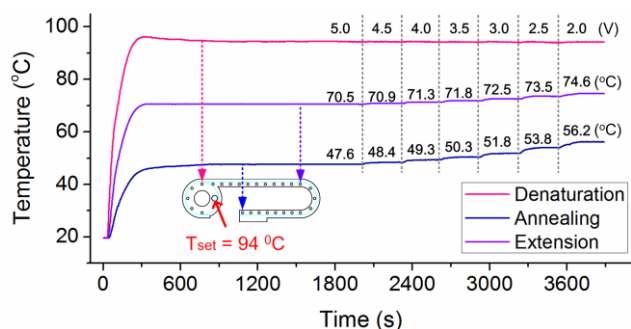
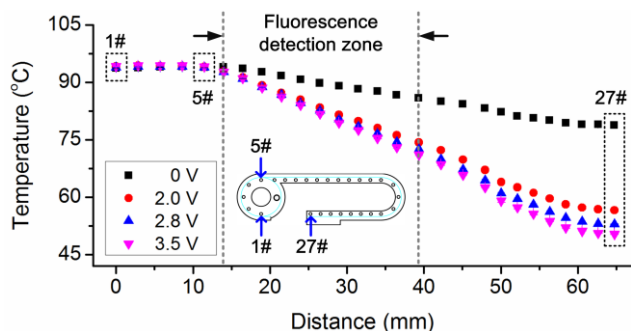


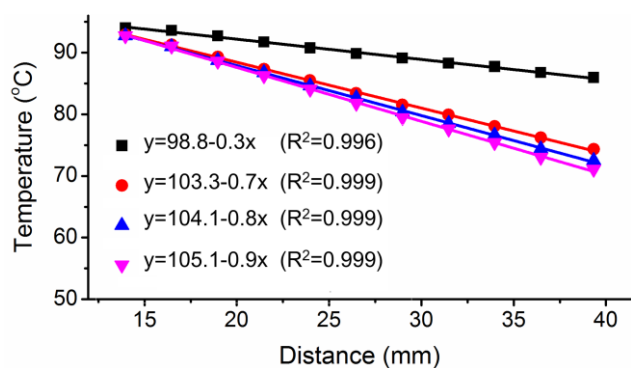
Figure 2. Operation principle of the FGAS.



(a)



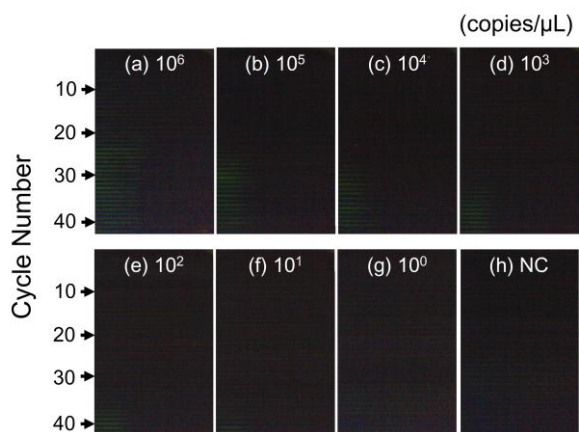
(b)



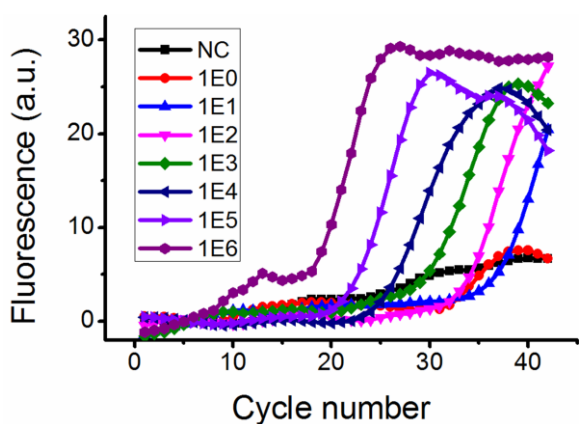
(c)

**Figure 3.** Evaluation of temperature response and thermal gradient on the microreactor of the FGAS. (a) Thermal time-responses of three representative points (as the dash arrows indicated) in denaturation, extension and annealing zones, with a single heater used to keep the temperature control point at  $94\text{ }^{\circ}\text{C}$  (as indicated by the solid arrow). By adjusting the applied voltages of the microfan from 5.0 V to 2.0 V, annealing temperatures in the range of  $47.6$  to  $56.2\text{ }^{\circ}\text{C}$  could be obtained. (b) Temperature distribution along the thermal gradient direction with varied applied voltages in case of 0 V (squares), 2.0 V (circles), 2.8 V (upright triangles), and 3.5 V (inverted triangles). (c) The linear regression fits of the data points

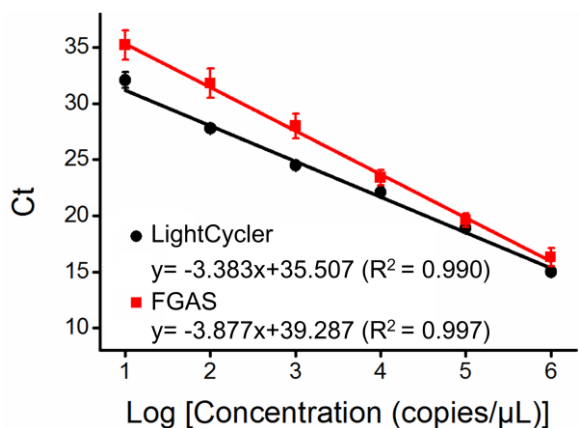
between two dash lines in the panel (b). Experimental errors less than  $\pm 0.1\text{ }^{\circ}\text{C}$  are smaller than symbols ( $n=3$ ).



(a)



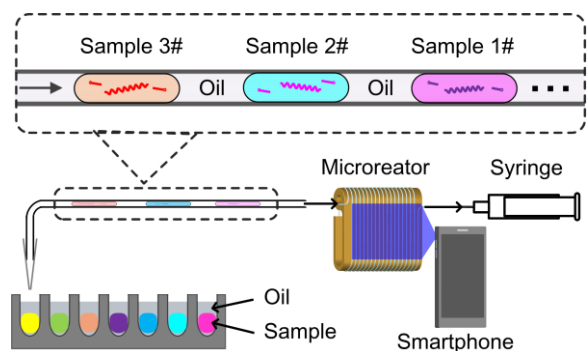
(b)



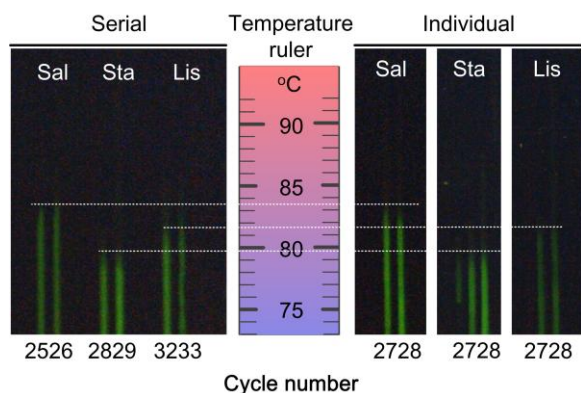
(c)

**Figure 4.** FGAS for real-time quantitative detection of genomic DNA of *Salmonella enterica*. (a) Representative combined fluorescence images (corresponded to sequential frames) of continuous-flow PCR amplicons amplified from DNA molecules of  $10^6$  to 0 copies/ $\mu\text{L}$ . (b) Amplification curves generated from the fluorescence images in (a). (c) Standard

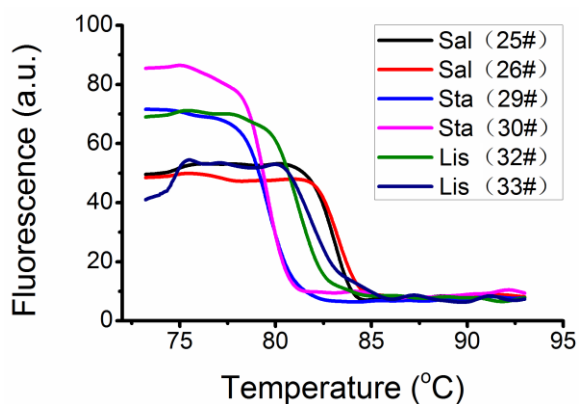
curves generated from the FGAS (red line) compared with those from the LightCycler (black line). Mean  $\pm$  s.d. ( $n=3$ ) of the threshold cycle (Ct) for the FGAS and the LightCycler were plotted against log of genomic DNA concentration. The red line is the linear regression fit ( $R^2 = 0.997$ ) of the Ct values from the FGAS, while the black line is the linear regression fit ( $R^2 = 0.990$ ) of the Ct values from the LightCycler.



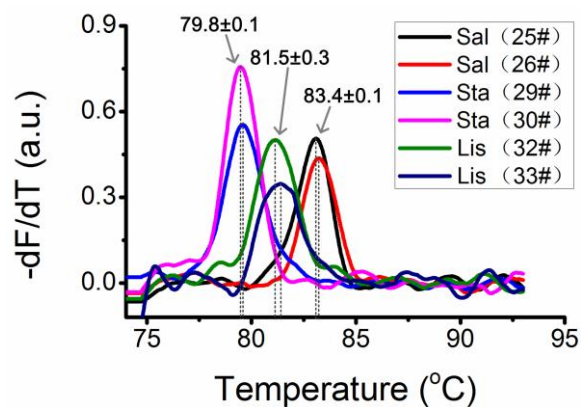
(a)



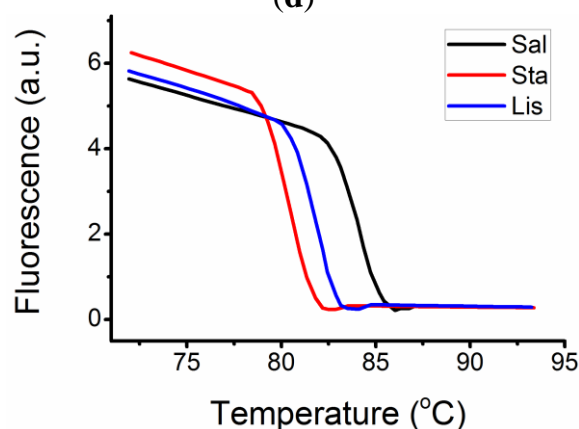
(b)



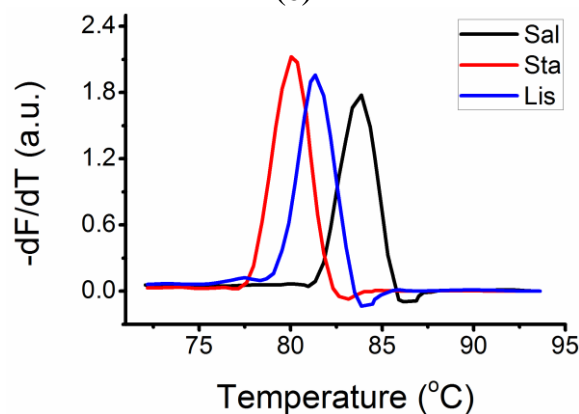
(c)



(d)

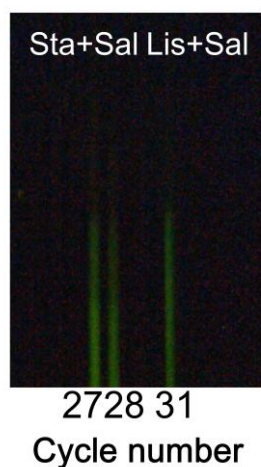


(e)

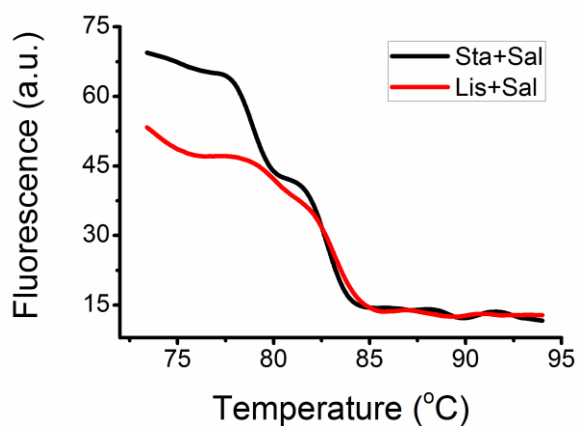


(f)

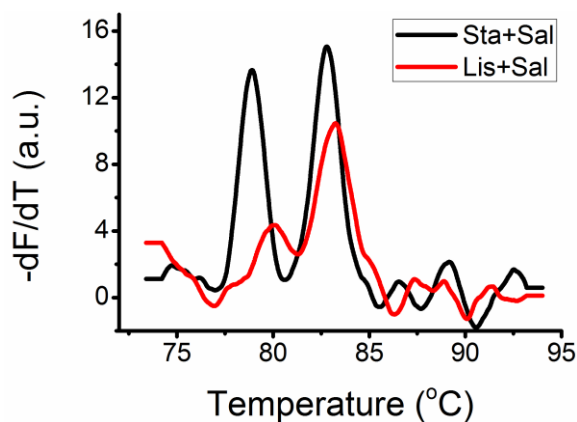
**Figure 5.** Serial identification of multiple DNAs using spatial melting-based multiplexed analysis with direct bar-chart readout on the FGAS. (a) Workflow for serial analysis of multiple samples. (b) Typical spatial melting fluorescence images of *Sal*, *Lis* and *Sta* DNAs in the serial (left) and individual (right) formats. (c-d) Melting curves and negative derivative plots of the products that were serially amplified on the FGAS. (e-f) Melting curves and negative derivative plots of the corresponding positive controls that were amplified on the Light Cycler.



(a)



(b)



(c)

amplifications were performed to detect the targets of “*Lis+ Sal*” and “*Sta +Sal*”. (b-c) Melting curves and negative derivative plots of products that were serially amplified on the FGAS. The plotted curves were smoothed using 1-degree Savitzky-Golay moving windows.

**Figure 6.** Serial and simultaneous multiplex amplification/detection on the FGAS that enabled serial continuous-flow multiplex PCR (SCF-MPCR) and multiplex spatial melting. (a) Typical fluorescence image of multiplex spatial melting during amplification on the FGAS. In the fluorescent channels, serial duplex